

Quenching of stable pulses in slow-fast excitable media.

Christopher D. Marcotte

*Department of Computer Science, Durham University, Durham, UK, DH1 3LE**

(Dated: April 25, 2024)

We develop linear theory for the prediction of excitation wave quenching—the construction of minimal perturbations which return stable excitations to quiescence—for localized pulse solutions of models of excitable media. The theory requires accounting for an additional degree of freedom in the formulation of the linear theory, and a reconsideration of heuristics for choosing optimal reference states from their group representation. We compare the predictions made with the linear theory to direct numerical simulations across a family of perturbations and assess the accuracy of predictions for models with distinct stable excitation structures. We find that the theory achieves qualitative predictive power with only the effort of distinguishing a root from the asymptotic case, and achieves quantitative predictive power in many circumstances. Finally, we compare the computational cost of our prediction technique to other numerical methods for the determination of transitions in extended excitable systems.

I. INTRODUCTION

Phenomenological and detailed ionic models of excitable media possess, at minimum, a stable rest state $\bar{\mathbf{u}}$ representing the quiescent state to which unstimulated tissue relaxes. Given the application of a sufficiently large (in amplitude and extent) perturbation to that rest state, the medium locally excites and extends the excited region by recruiting the energy stored in the quiescent excitable medium ahead of the front. These fronts may persist indefinitely or the medium may recover in finite time, so that the front develops into a localized pulse which *transiently* recruits the energy of the medium. Front or pulse solutions are center-stable traveling wave solutions of the underlying partial differential equation (PDE) model of the medium dynamics, and the minimal perturbation which stably transitions the system from the rest state to the excited state is the critical ignition perturbation. Likewise, the minimal perturbation which stably transitions the system from the excited state to the rest state is the critical *quenching* perturbation.

If we understand cardiac arrhythmia as the presence of undesirable excitations in the heart muscle, then the development of defibrillation techniques are targeted investigations of quenching in a specific context (i.e. cardiac arrhythmia with uncertain states). The literature covering suppression of cardiac excitation waves is vast, c.f. Ref. 1 and citations therein. Numerous methods are presented in the mathematical, rather than medical, literature, as well. [2–4]. The suppression of stable traveling waves in lower dimensional settings is less well-studied. Ref. 5 investigated the quenching (‘successful suppression’) of stable pulses in slow-fast excitable media through the application of a time-dependent control to the slow variable; they formalize this approach as the

imposition of a lag on the wavefront such that the distance between the wavefront and the waveback of the excitation shrinks to zero in finite time. This approach makes intuitive sense, and reflects one of the dominant pathways for wave break observed in models of cardiac electrical excitation [6]. However, this approach may only work for *pulse* solutions, and may over-suppress for models with realistic dissipation of waves expected to be relevant for cardiac electrical excitations. [7]

Throughout this manuscript, models of excitable media will take the form of a reaction-diffusion PDE,

$$\partial_t \mathbf{u} - \mathbf{D} \partial_x^2 \mathbf{u} = \mathbf{f}(\mathbf{u}), \quad (1)$$

where $\mathbf{u} = [u_1, \dots, u_m](t, x)$ and $\mathbf{f} = [f_1, \dots, f_m]$. The diffusion parameters $\mathbf{D} = \text{diag}(1, 0, \dots)$ restrict diffusion to the fast channel, u_1 , requiring that the remaining components are non-diffusive. The excitable system has a unique spatially uniform rest state denoted $\bar{\mathbf{u}}$, which satisfies $\mathbf{f}(\bar{\mathbf{u}}) = \mathbf{0}$, from which the ignition of excitations has been investigated previously [8–16]. In a frame moving with speed c , eq. (1) becomes

$$\mathbf{0} = \mathbf{D} \mathbf{u}'' + c \mathbf{u}' + \mathbf{f}(\mathbf{u}), \quad (2)$$

where $\mathbf{u}' = d\mathbf{u}/d\xi$, and $\xi = x - ct$. For sufficiently large domains, two solutions of (2) persist for $c > 0$, with the slower ($c = \hat{c} < \check{c}$) corresponding to an unstable traveling wave solution ($\hat{\mathbf{u}}$) and the faster ($c = \check{c} > \hat{c}$) corresponding to a stable traveling wave solution ($\check{\mathbf{u}}$). [17] When the slow wave has a single unstable mode, the center-stable manifold separates the stable rest state from the stable wave configuration in the whole state space.

Linearizing about a reference unstable wave solution defines the comoving-frame linearized operator and the corresponding left and right eigenmodes,

$$\hat{\mathbf{v}}_i \sigma_i = \mathcal{L}(\hat{\mathbf{u}}, \hat{c}) \hat{\mathbf{v}}_i, \quad \hat{\mathbf{w}}_j^\dagger \sigma_j^* = \mathcal{L}^\dagger(\hat{\mathbf{u}}, \hat{c}) \hat{\mathbf{w}}_j^\dagger, \quad (3)$$

such that the left eigenfunctions ($\hat{\mathbf{w}}_i$) are the unique projectors of the right eigenfunctions ($\hat{\mathbf{v}}_i$). Though the

* Corresponding author: christopher.marcotte@durham.ac.uk

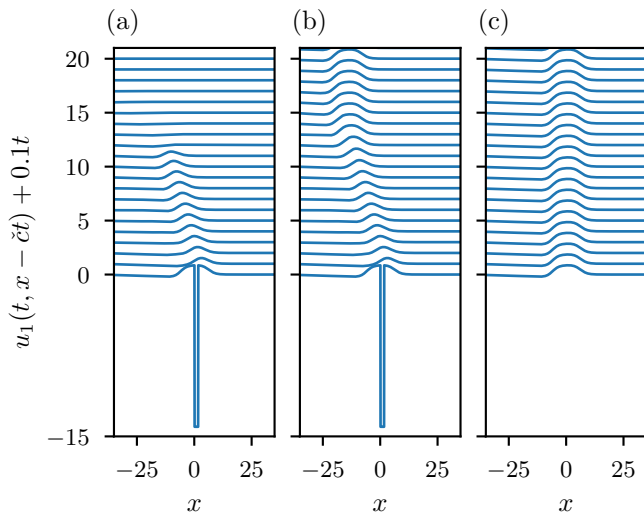


FIG. 1. (a) Supercritical, (b) subcritical, and (c) unperturbed dynamics for the FitzHugh-Nagumo model in frame moving with speed \tilde{c} . For (a,b), the quenching perturbation is a rectangular envelope in the u_1 channel, centered at $x = 1$, with width substantially smaller than the pulse, and amplitudes $U_{q\pm} = -18.8314 \mp 10^{-4}$ for the super- and sub-critical perturbations, respectively.

solutions of (3) are formally scale-free, the left and right sets of eigenfunctions satisfy an orthonormality condition using the inner product, $\delta_{ij} = \langle \hat{\mathbf{w}}_j | \hat{\mathbf{v}}_i \rangle = \int_{-\infty}^{+\infty} d\xi \hat{\mathbf{w}}_j^\dagger(\xi) \hat{\mathbf{v}}_i(\xi)$. The eigenvalues, σ_i , determine the growth of each eigenmode $\hat{\mathbf{v}}_i$ over time. Generically, $\mathcal{L}(\hat{\mathbf{u}}, \hat{c})$ is not self-adjoint, and the left and right eigenfunctions are distinct, and $\sigma_1 > 0$ while $\sigma_2 = 0$.

Figure 1(a) demonstrates quenching; for super-critical amplitude perturbations to the stable excitation wave, the state approaches quiescence, $\lim_{t \rightarrow \infty} \mathbf{u}(t, x) \rightarrow \bar{\mathbf{u}}$. For sub-critical amplitude perturbations the stable excitation wave recovers, shown in figure 1(b). The sub-critical perturbation has the net effect of introducing some lag $\delta > 0$ in the progression of wave relative to the unperturbed stable excitation wave, c.f., figure 1(b,c), $\lim_{t \rightarrow \infty} \mathbf{u}(t, x) \rightarrow \check{\mathbf{u}}(x - \tilde{c}t - \delta)$.

II. THEORY

In this section we develop the theoretical groundwork for the methods used in this paper. We first describe the essential ingredients of the classical linear ignition theory, and unify the methods for selecting a representative from the translational symmetry group using heuristics motivated by notions of distance in infinite-dimensional spaces. We then extend the ignition theory to non-uniform stable states and detail the computation of the critical amplitude in this new context. The final portion of this Section derives and simplifies the analogous heuristics from the linear ignition theory for the quenching problem, and develops a uniqueness argument based

on the asymptotic properties of the perturbation.

A. Ignition

The classical ignition problem[12, 14, 15] considers the critical perturbation to the quiescent state for which the dynamics asymptotically approaches the stable excitation wave. Identifying the initial condition $\mathbf{u}(0, x) = \mathbf{u}_0(x)$ as a perturbation from the rest state $\bar{\mathbf{u}}(x) + U(s)\bar{\mathbf{X}}(x)$ and equating this configuration to a perturbed reference state selected from the group orbit of the unstable wave, $\hat{\mathbf{u}}(\xi) + \hat{\mathbf{h}}(\xi)$, where $\xi = x - s$ and s an appropriate shift,

$$\mathbf{u}_0(x) = \hat{\mathbf{u}}(\xi) + \hat{\mathbf{h}}(\xi) = \bar{\mathbf{u}}(x) + U(s)\bar{\mathbf{X}}(x), \quad (4)$$

allows us to use information about the exact solution $\hat{\mathbf{u}}(\xi)$ to predict the long-term dynamics of $\mathbf{u}_0(x)$. Using the linearization about the reference state, we may predict the minimal amplitude of a localized perturbation to the rest state which successfully “ignites” the medium by taking an appropriate inner product with $\hat{\mathbf{w}}_1(\xi)$ and requiring the excitation of the unstable mode to vanish. As the rest state is (typically) uniform and invariant with respect to translations, and the unstable wave is equivariant under translations, we must select a reference frame from the group representation, parameterized by a shift s . Rearranging this constraint gives a compact equation for the critical ignition amplitude for a prescribed perturbation envelope,

$$\bar{U}(s) = \frac{\langle \hat{\mathbf{w}}_1(\xi) | \hat{\mathbf{u}}(\xi) - \bar{\mathbf{u}} \rangle}{\langle \hat{\mathbf{w}}_1(\xi) | \bar{\mathbf{X}}(\xi + s) \rangle}, \quad (5)$$

where the appropriate shift s is determined by a constraint equation, $0 = \langle \bar{\Phi}_l(\xi) | \bar{\mathbf{X}}(\xi + s) \rangle$. The constraint functional $\bar{\Phi}_l(\xi)$ derives from heuristic considerations for the optimal reference frame, which we will return to for the application to quenching later in this Section. We include the frame selectors for the classical ignition problem for completeness,

$$\begin{aligned} \bar{\Phi}_1(\xi) &= \langle \hat{\mathbf{w}}_1 | \hat{\mathbf{u}} - \bar{\mathbf{u}} \rangle \hat{\mathbf{w}}_1'(\xi), \\ \bar{\Phi}_2(\xi) &= \langle \hat{\mathbf{w}}_1 | \hat{\mathbf{u}} - \bar{\mathbf{u}} \rangle \hat{\mathbf{v}}_2(\xi) - \langle \hat{\mathbf{v}}_2 | \hat{\mathbf{u}} - \bar{\mathbf{u}} \rangle \hat{\mathbf{w}}_1(\xi), \\ \bar{\Phi}_3(\xi) &= \langle \hat{\mathbf{w}}_1 | \hat{\mathbf{u}} - \bar{\mathbf{u}} \rangle \hat{\mathbf{w}}_2(\xi) - \langle \hat{\mathbf{w}}_2 | \hat{\mathbf{u}} - \bar{\mathbf{u}} \rangle \hat{\mathbf{w}}_1(\xi), \end{aligned}$$

noting that each $\bar{\Phi}_l(\xi)$ is formed explicitly from the available rest-state, unstable wave, and the leading left and right eigenfunctions of the unstable wave. The constraint equation may be expressed as a function of the shift alone, $\bar{\mu}_l(s) = \langle \bar{\Phi}_l(\xi) | \bar{\mathbf{X}}(\xi + s) \rangle$, where the inner product is evaluated over all x by the cross-correlation integral of two vector functions with an implicit sum over the variable indices. The critical excitation frame is determined by an appropriate root, $\bar{\mu}_l(s^*) = 0$, which can be assumed unique based on the slow-fast scaling of the left and right eigenfunctions [16]. We will now adapt the detailed critical ignition argument for the quenching context.

B. Quenching

When considering $\check{\mathbf{u}}(x)$ in place of $\bar{\mathbf{u}}$, the construction of frame-determining functions requires additionally considering the variation of the original state. When the state is uniform, the perturbation may always be arbitrarily shifted to the same coordinate frame as the state; when the state is non-uniform, the perturbation has an induced parametric shift in frame, denoted θ , which describes the origin of the perturbation. Given a stable moving solution, $\mathbf{u}(t, x) = \check{\mathbf{u}}(x - \check{c}t)$, and an unstable moving solution $\mathbf{u}(t, x) = \hat{\mathbf{u}}(x - \hat{c}t)$, we can consider an initial configuration $\mathbf{u}(0, x) = \mathbf{u}_0(x)$ expressed as a perturbation to the stable solution,

$$\mathbf{u}_0(x) = \check{\mathbf{u}}(x) + \check{\mathbf{h}}(x - \theta; x_s),$$

and predict whether the initial configuration will relax to the rest state $\mathbf{u}(t, x) \rightarrow \bar{\mathbf{u}}$ as $t \rightarrow \infty$.

The linear theory considers the linearization about the unstable solution, selected from along its group orbit, $\exp(+t\hat{c}\partial_x)\hat{\mathbf{u}}(x - \hat{c}t - s) = \hat{\mathbf{u}}(x - s)$ for all times $t \geq 0$. We rewrite the initial configuration as the unstable solution plus a perturbation,

$$\mathbf{u}(t, x) = \hat{\mathbf{u}}(x - s) + \check{\mathbf{u}}(x) + \check{\mathbf{h}}(x - \theta; x_s) - \hat{\mathbf{u}}(x - s),$$

which identifies $\hat{\mathbf{h}}(x - s) = \check{\mathbf{u}}(x) + \check{\mathbf{h}}(x - \theta; x_s) - \hat{\mathbf{u}}(x - s)$. The construction of the theory is such that markedly different slow and fast waves limit the accuracy of the perturbation argument. Linearizing about $\hat{\mathbf{u}}(x - s)$ and computing the excitation of the leading eigenmode at time $t = 0$,

$$a_1(0) = \langle \hat{\mathbf{w}}_1(x - s) | \check{\mathbf{u}}(x) - \hat{\mathbf{u}}(x - s) + \check{\mathbf{h}}(x - \theta; x_s) \rangle,$$

we require $a_1(0) = 0$ to vanish, so to as to not excite the unstable mode, i.e. criticality. Rearranging, we find

$$\langle \hat{\mathbf{w}}_1(x - s) | \check{\mathbf{h}}(x - \theta; x_s) \rangle = \langle \hat{\mathbf{w}}_1(x - s) | \hat{\mathbf{u}}(x - s) - \check{\mathbf{u}}(x) \rangle.$$

Defining $\check{\mathbf{h}}(x - \theta; x_s) = U(s; \theta, x_s)\check{\mathbf{X}}(x - \theta; x_s)$ gives a parametric expression for the critical amplitude of the perturbation in s and θ ,

$$\check{U}(s; \theta, x_s) = \frac{\langle \hat{\mathbf{w}}_1(\xi) | \hat{\mathbf{u}}(\xi) - \check{\mathbf{u}}(\xi + s) \rangle}{\langle \hat{\mathbf{w}}_1(\xi) | \check{\mathbf{X}}(\xi + s - \theta; x_s) \rangle} \quad (6)$$

Compare (6) with (5), and the explicit coordinate parameter θ becomes interpretable as a relative phase for the perturbation along the stable wave. This expression is a function of the reference frame shift s , and parameterized by the perturbation envelope center θ and width x_s .

Selecting appropriate reference frame shifts given non-uniform initial states requires a reassessment of the underlying assumptions of the derivation of the frame selection heuristics. We now apply each heuristic to derive the quenching problem shift selectors, $\check{\Phi}_l(\xi, s)$, which define the reference frame as the root of a parameterized inner product with the perturbation, i.e. $\check{\mu}_l(s^*) = 0$.

In the ignition case, the first heuristic minimizes the amplitude of the perturbation to $\bar{\mathbf{u}}(x)$ over all frames s by extremizing the numerator of (5). This approach relies on $\partial_s \langle \hat{\mathbf{w}}_1(x - s) | \hat{\mathbf{u}}(x - s) - \bar{\mathbf{u}} \rangle = 0$, due to $\partial_x \bar{\mathbf{u}}(x) = \mathbf{0}$ (i.e. $\mathbf{u}_0(x) = \bar{\mathbf{u}}$). For ignition the condition simplifies to, $0 = \langle \hat{\mathbf{w}}_1'(x - s) | \check{\mathbf{h}}(x - s) \rangle$. For the quenching problem, $\partial_x \check{\mathbf{u}}(x) \neq \mathbf{0}$, the minimization of $U(s; \theta, x_s)$ with respect to s is determined by $0 = \partial_s U(s; \theta, x_s)$, whose numerator expands to,

$$0 = \langle \hat{\mathbf{w}}_1(x - s) | \hat{\mathbf{u}}(x - s) - \check{\mathbf{u}}(x) \rangle \langle \hat{\mathbf{w}}_1'(x - s) | \check{\mathbf{h}}(x - \theta; x_s) \rangle \\ - \langle \hat{\mathbf{w}}_1(x - s) | \check{\mathbf{h}}(x - \theta; x_s) \rangle (\langle \hat{\mathbf{w}}_1'(x - s) | \hat{\mathbf{u}}(x - s) - \check{\mathbf{u}}(x) \rangle \\ + \langle \hat{\mathbf{w}}_1(x - s) | \hat{\mathbf{u}}'(x - s) \rangle).$$

Rearranging to form $\check{\Phi}_1(x - s; s)$,

$$\check{\Phi}_1(x - s; s) = \langle \hat{\mathbf{w}}_1(x - s) | \hat{\mathbf{u}}(x - s) - \check{\mathbf{u}}(x) \rangle \hat{\mathbf{w}}_1'(x - s) \\ - \langle \hat{\mathbf{w}}_1'(x - s) | \hat{\mathbf{u}}(x - s) - \check{\mathbf{u}}(x) \rangle \hat{\mathbf{w}}_1(x - s),$$

where we have used $\langle \hat{\mathbf{w}}_1(x - s) | \hat{\mathbf{u}}'(x - s) \rangle = \langle \hat{\mathbf{w}}_1(x - s) | \hat{\mathbf{v}}_2(x - s) \rangle = 0$, guaranteed by the biorthogonality of the eigenmodes. Here we note the first major divergence from the ignition problem formalism, where $\check{\Phi}_l(x - s; s)$ transforms with s as the product of vectors with $(x - s)$ dependence weighted by scalars with s dependence,

$$\check{\Phi}_l(x - s; s) = \phi_{l,1}(s)\mathbf{a}_{l,1}(x - s) + \phi_{l,2}(s)\mathbf{a}_{l,2}(x - s). \quad (7)$$

This change in the transformation of $\check{\Phi}_l(x - s; s)$ from the ignition formalism informs a new approach to frame selection.

The second heuristic minimizes the L_2 -distance between the perturbed solution and the unstable reference solution over all choices of frame parameterized by the shift s ,

$$s_2 = \arg \min_s \langle \mathbf{u}(x) - \hat{\mathbf{u}}(x - s) | \mathbf{u}(x) - \hat{\mathbf{u}}(x - s) \rangle,$$

for which a necessary condition is that the L^2 norm of $\mathbf{u}(x) - \hat{\mathbf{u}}(x - s)$ is extremal, i.e. $\partial_s \langle \mathbf{u}(x) - \hat{\mathbf{u}}(x - s) | \mathbf{u}(x) - \hat{\mathbf{u}}(x - s) \rangle^2 = 0$, which simplifies using $\hat{\mathbf{v}}_2(x - s) = -\partial_s \hat{\mathbf{u}}(x - s)$,

$$0 = \langle \hat{\mathbf{v}}_2(x - s) | \check{\mathbf{u}}(x) + \check{\mathbf{h}}(x - \theta; x_s) - \hat{\mathbf{u}}(x - s) \rangle,$$

from which we rearrange to identify $\check{\Phi}_2(x - s; s)$,

$$\check{\Phi}_2(x - s; s) = \langle \hat{\mathbf{w}}_1(x - s) | \hat{\mathbf{u}}(x - s) - \check{\mathbf{u}}(x) \rangle \hat{\mathbf{v}}_2(x - s) \\ - \langle \hat{\mathbf{v}}_2(x - s) | \hat{\mathbf{u}}(x - s) - \check{\mathbf{u}}(x) \rangle \hat{\mathbf{w}}_1(x - s).$$

The third heuristic requires that the perturbation be orthogonal to the space spanned by the first and second right eigenfunctions; as the first eigenmode appears in the constraint in the derivation of (6), this is satisfied by the projection onto the second left eigenmode, i.e. the translational response function,

$$0 = \langle \hat{\mathbf{w}}_2(x - s) | \check{\mathbf{u}}(x) + \check{\mathbf{h}}(x - \theta; x_s) - \hat{\mathbf{u}}(x - s) \rangle,$$

which may be rearranged to form $\check{\Phi}_3(x-s; s)$,

$$\check{\Phi}_3(x-s; s) = \langle \hat{\mathbf{w}}_1(x-s) | \hat{\mathbf{u}}(x-s) - \check{\mathbf{u}}(x) \rangle \hat{\mathbf{w}}_2(x-s) - \langle \hat{\mathbf{w}}_2(x-s) | \hat{\mathbf{u}}(x-s) - \check{\mathbf{u}}(x) \rangle \hat{\mathbf{w}}_1(x-s),$$

which we identify as $\check{\Phi}_2(x-s; s)$ where the second right eigenfunction ($\hat{\mathbf{v}}_2(\xi)$) is replaced with its projector ($\hat{\mathbf{w}}_2(\xi)$).

The shift selectors $\check{\Phi}_l(x-s; s)$ are thus vector-valued functions of $\xi = x-s$ which transform nonlinearly with s . The utility of the projector formalism is thus limited, and for simplicity, we form the scalar functions

$$\check{\mu}_l(s; \theta, x_s) = \langle \check{\Phi}_l(x-s; s) | \check{\mathbf{X}}(x-\theta; x_s) \rangle, \quad (8)$$

which reduces over the spatial coordinate x and the variable index, and whose root(s) define potential reference frame(s) for a particular perturbation. The question of identifying a *unique* frame amounts to selecting a *single* root of (8).

Indeed, we have no strong guarantees for the uniqueness of the roots, for the general case. We may, however, motivate a procedure which guarantees a unique root for all x_s provided a unique root exists for $x_s \rightarrow \infty$. We assume the perturbation envelope is parameterized such that it asymptotically approaches a constant vector of length m with unit L^∞ -norm,

$$\lim_{x_s \rightarrow \infty} \|\check{\mathbf{X}}(x-\theta; x_s)\|_\infty \rightarrow 1,$$

and implying $\partial_\theta U(s; \theta, x_s) = \partial_{x_s} U(s; \theta, x_s) = 0$ in the limit. For expositional simplicity, we assume that the asymptotically wide perturbation is entirely in the u_1 -channel of the state, i.e. $\lim_{x_s \rightarrow \infty} \check{\mathbf{X}}(x-\theta; x_s) \rightarrow [1, 0, \dots]$. In the asymptotic regime, we thus require a means of identifying a unique root s^* of (8), which we take to be the most strongly negative option of (6). For $\lim_{x_s \rightarrow \infty} U(s; \theta, x_s) < 0$, we require,

$$\langle \hat{\mathbf{w}}_1(\xi) | \hat{\mathbf{u}}(\xi) - \check{\mathbf{u}}(\xi+s) \rangle \langle \hat{\mathbf{w}}_1(\xi) | \check{\mathbf{X}}(\xi+s-\theta; x_s) \rangle < 0.$$

The second factor can be guaranteed positive due to the biorthogonality of the eigenfunctions, and the first may be asserted negative based on the construction of the slow and fast waves and the triangle inequality; we may select a shift s which extremizes $\langle \hat{\mathbf{w}}_1(\xi) | \check{\mathbf{u}}(\xi+s) \rangle$ while leaving $\langle \hat{\mathbf{w}}_1(\xi) | \hat{\mathbf{u}}(\xi) \rangle$ constant. Given the asymptotic solution $\lim_{x_s \rightarrow \infty} U(s; \theta, x_s)$, we may trace the branch of solutions to smaller perturbation widths until the solution vanishes, and thus construct a unique prediction for the critical quenching amplitude through continuation.

We have published example code and data for the linear theory prediction of critical quenching perturbations online [18]. This code only requires the location of files containing $\bar{\mathbf{u}}$, $\check{\mathbf{u}}$, $\hat{\mathbf{u}}$, and $\hat{\mathbf{v}}_1$, $\hat{\mathbf{v}}_2$, $\hat{\mathbf{w}}_1$, and $\hat{\mathbf{w}}_2$, on a consistent domain. The code performs estimation of the error of the method by comparing the construction of $\check{\mu}_l(s; \theta, x_s)$ against $\langle \check{\Phi}_l(x-s; s) | \check{\mathbf{X}}(x-\theta) \rangle$, where the $\check{\Phi}_l(x-s; s)$ is computed by explicit translation of the vector components.

III. METHODS

The essential ingredients of the application of the extended linear theory to a prescribed perturbation envelope $\check{\mathbf{X}}(x-\theta; x_s)$, are the stable solution $\check{\mathbf{u}}$, the unstable solution, $\hat{\mathbf{u}}$, the leading two left eigenfunctions $\hat{\mathbf{w}}_1$ & $\hat{\mathbf{w}}_2$, and their associated derivatives. The solutions themselves are computed approximately using continuation within the AUTO-07P [19] framework. The solutions are then refined to a tighter tolerance using a global spectral expansion, and the refined solutions used as non-constant-coefficient fields in the forward and adjoint eigenproblems within the DEDALUS2 [20] framework. From these quantities, any of the $\check{\mu}_l(s; \theta, x_s)$ may be formed by computing cross-correlation integrals, likewise the prediction of $\check{U}(s; \theta, x_s)$ using the formalism laid out in the previous section.

To verify the linear theory predictions, we form initial conditions parameterized by perturbation amplitude $U_q(\theta, x_s) < 0$, width x_s , and position θ ,

$$\mathbf{u}_0(x) = \check{\mathbf{u}}(x) + U_q(\theta, x_s) \check{\mathbf{X}}(x-\theta; x_s).$$

For the purposes of testing the predictions of the linear theory, the perturbation is defined by a top-hat function centered at θ ,

$$\check{\mathbf{X}}(y; x_s) = [1, 0, \dots] H(y+x_s/2) H(x_s/2-y), \quad (9)$$

where where $y = x-\theta$ and $H(z) = (1+\text{sign}(z))/2$ approximates the Heaviside distribution. The shape is defined such that $\|\check{\mathbf{X}}_1(x-\theta; x_s)\|_\infty = 1$ and $\|\check{\mathbf{X}}_1(x-\theta; x_s)\|_1 = x_s$, so that the perturbation is strictly in the fast (voltage) variable. While this choice of perturbation shape is chosen for its simplicity it is not unique the methods described in this work are not specific to this parameterization.

We solve the initial-boundary-value problem (1) with initial condition $\mathbf{u}_0(x)$ and periodic boundary conditions over $x \in [0, L]$ and a fixed time interval, e.g. $t \in [0, T]$ with $T = L/(2\check{c})$, using the DEDALUS2 framework initial-value problem (IVP) solver. [21] We simultaneously track the state over time, $\mathbf{u}(t, x)$, and compare the final state, using an appropriate measure, to the exact solutions. This procedure amounts to the solution of a one-dimensional root-finding problem for each width and shift pair for the critical quenching amplitude.

We track the development of the perturbed stable wave over time by computing the absolute-valued deviation of the fast variable from the rest state,

$$\psi(t) = \int_0^L dx |u_1(t, x) - \bar{u}_1|, \quad (10)$$

and compare the final value $\psi(T)$ to the respective evaluation at \bar{u}_1 , \hat{u}_1 , and \check{u}_1 , which we designate by $\hat{\psi} \equiv 0$, $\hat{\psi}$, and $\check{\psi}$, respectively. The critical amplitude is then defined by the root of the function,

$$\varphi(U_q) = \lim_{t \rightarrow \infty} \psi(t; U_q) - \hat{\psi}, \quad (11)$$

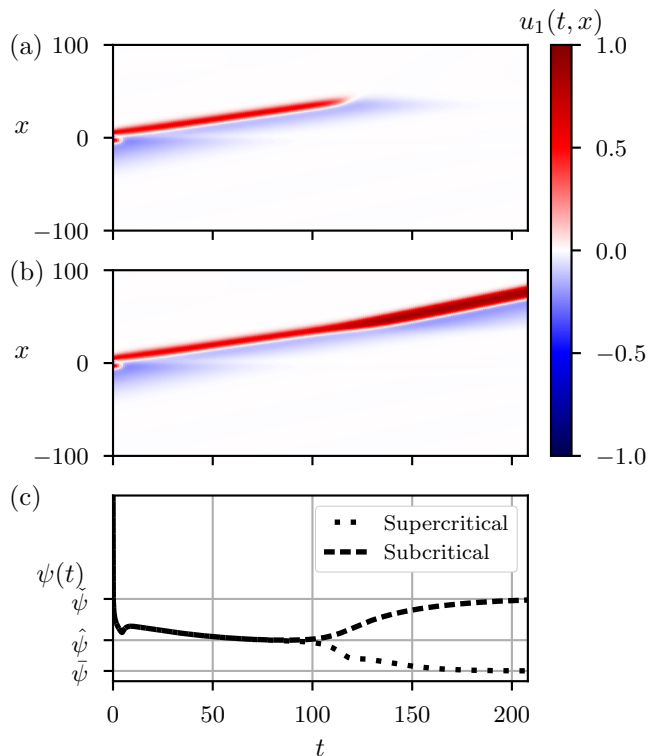


FIG. 2. (a) Super-critical and (b) sub-critical dynamics of the FitzHugh-Nagumo model (12) corresponding to figure 1(a,b), represented as spacetime diagrams of the fast variable $u_1(t, x)$ and (c) their diagnostic function $\psi(t)$ for the (dots) super-critical and (dash) sub-critical dynamics.

where $\lim_{t \rightarrow \infty} \psi(t; U_q) \in \{\bar{\psi}, \hat{\psi}, n\check{\psi} - (n-1)\check{\delta}\}$ where the last option accounts for the possibility of transient back-ignition ($n \in \mathbb{N}$ denotes the number of stable pulses) and $\check{\delta}$ is the overlap deformation correction to $\psi(T)$ from the presence of multiple stable pulses on the same domain. As $T \rightarrow \infty$, the probabilities of $\varphi(U_q)$ taking on these values approaches $\{P_q, 0, 1 - P_q\}$, where P_q is the probability that U_q is quenching for a provided (x_s, θ) pair. While no diagnostic function is able to uniquely determine the ultimate attractor of any arbitrarily configured state, in a large neighborhood centered on each of the exact stable solutions, this intuition holds. We ensure that our final states are in such a neighborhood by solving the IVP over a sufficiently long time interval.

Figure 2(a,b) depicts the super- and sub-critical dynamics for the quenching perturbations along with (c) their diagnostic function $\psi(t)$. While $\psi(0)$ is very close between the two solutions, $|\psi_-(0) - \psi_+(0)| \approx |(U_q^- - U_q^+)x_s| = 3 \times 10^{-4}$, they diverge after $t \approx 100$, which corresponds to the close passage of the state to the unstable pulse solution, $\hat{\mathbf{u}}$, and corresponding measure $\hat{\psi}$. After $t \approx 200$, the two solutions have diverged and are very similar to the two stable states, $\bar{\mathbf{u}}$ and $\check{\mathbf{u}}$, in (a,b), respectively. Further refinement of the critical perturbation amplitude for this (x_s, θ) pair may be attained using a bisection root-finding algorithm, limited only by

the local error of the time-stepping procedure.

IV. RESULTS

In this Section, we first introduce an excitable model, and remark on its inclusion and relevance to the task at hand. We proceed to describe the relevant linear theory ingredients and the efficacy of these ingredients in predicting the minimum threshold amplitude for excitation, across a range of perturbation widths and positions. We finish the discussion of each model by comparing the DNS results and linear theory predictions, and the successes and limitations of the latter for predicting the former.

A. FitzHugh-Nagumo model

The FitzHugh-Nagumo is an archetypical model of excitable media which arises from a simplification of squid axon signal dynamics [22]. The reliability of the model for cardiac dynamics is tenuous, but remains an essential testbed for new approaches to the study of the fundamental properties of excitation waves. The model consists of two non-dimensional state variables interacting in a slow-fast system,

$$f_1 = u_1(1 - u_1)(u_1 - \beta) - u_2, \quad f_2 = \gamma(\alpha u_1 - u_2), \quad (12)$$

where we identify u_1 as the fast component and u_2 as the slow component, based on the time-scale separation $\gamma \ll 1$. For the purposes of this study we fix $\alpha = 0.37$ and $\beta = 0.131655$, and vary γ , to consider morphologies of the fast and slow waves which are aligned with and counter to the underlying assumptions of the linear method. We choose the time-scale separation $\gamma \in \{0.001, 0.010, 0.020, 0.025\}$ to explore differences in the morphology of the fast and slow pulses, c.f. fig. 3 & fig. 4, respectively. In the limit of $\gamma \rightarrow 0$, the slow pulse speed vanishes, $\lim_{\gamma \rightarrow 0} \hat{c} \rightarrow 0$, forming a critical nucleus; meanwhile, in the same limit, the fast pulse loses post-excitation recovery, developing into a stable propagating front with finite speed $\lim_{\gamma \rightarrow 0} \check{c} > 0$. As γ increases from 0, the fast and slow waves converge until coincidence for $\gamma_c \approx 0.026$.

Figure 3 depicts periodic stable pulse solution for each choice of γ over the nullclines of the model. Each stable solution is interpolated using $M = 4096$ Chebyshev modes on a periodic domain of length $L = 2700$ with dealiasing factor $N/M = 2$. These solutions are resolved with projective boundary conditions and approximately homoclinic to $O(10^{-13})$. To our knowledge there exists no generally applicable exact solution for the fast pulse on unbounded domains with non-vanishing slow-fast time-scale separation parameter [23], but appropriate asymptotics hold approximately [17].

The scaling of the critical pulse and the leading eigenmodes was investigated in a previous work [16], which is

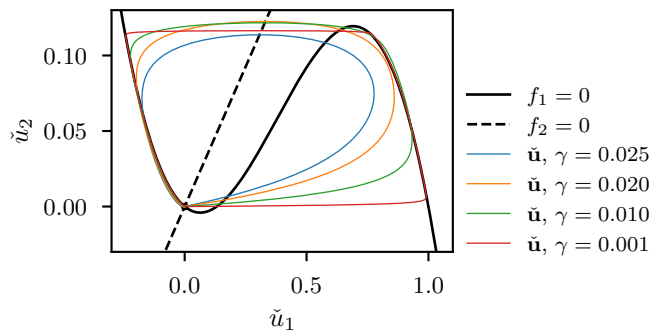


FIG. 3. Nullclines of the FitzHugh-Nagumo model (black; $f_1 = 0$ solid, $f_2 = 0$ dashed) and the stable pulse solutions for $\gamma \in \{0.025, 0.020, 0.010, 0.001\}$.

most relevant for $\gamma \rightarrow 0$. In the range $10^{-3} \leq \gamma < \gamma_c$, the scaling of the components of the pulse and eigenmodes change slowly, but the components of the pulse and eigenmodes change shape significantly as γ varies. The unstable solutions and their associated eigenfunctions are resolved with $M = 4096$ Chebyshev modes on a domain of length $L = 1500$ with dealiasing factor $N/M = 2$, which is sufficient to resolve the fast and slow components of the solution to approximately 10^{-13} in L^∞ -norm for the solutions presented here. The linear theory ingredients are depicted in figure 4. The pulses are oriented such that the peak of the fast component occurs precisely at the origin: $0 = \arg \max \hat{u}_1(x)$, for all γ , matching the orientation of the fast pulse solutions ($0 = \arg \max \check{u}_1(x)$).

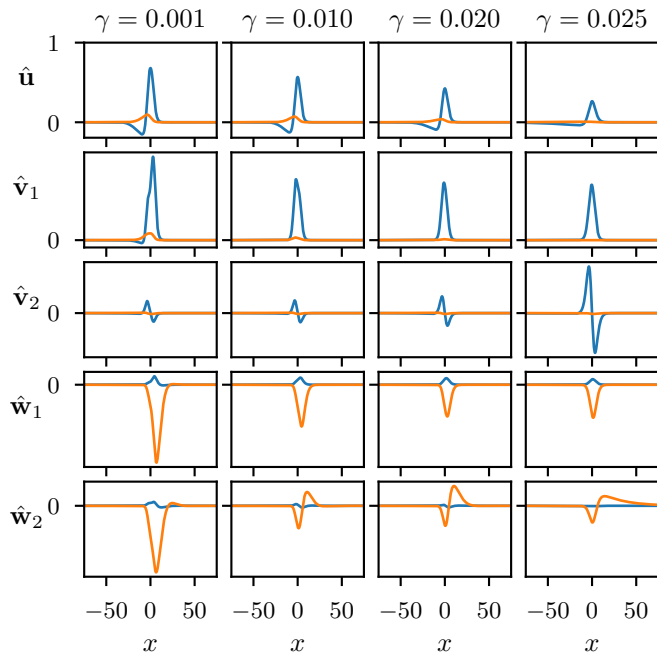


FIG. 4. Linear theory ingredients for the FitzHugh-Nagumo model. (Top row) Unstable pulse solution $\hat{\mathbf{u}}$ for $\gamma \in \{0.001, 0.010, 0.020, 0.025\}$, with (second row) $\hat{\mathbf{v}}_1$, (third row) $\hat{\mathbf{v}}_2$, (fourth row) $\hat{\mathbf{w}}_1$, and (fifth row) $\hat{\mathbf{w}}_2$.

The left and right eigenfunctions are depicted such that the appropriate pairs satisfy $\langle \hat{\mathbf{w}}_i | \hat{\mathbf{v}}_i \rangle = 1$ for $i = 1, 2$, and oriented such that $\hat{v}_1^{(1)}(0) > 0$ and $\partial_x \hat{v}_2^{(1)}(0) < 0$, for visual consistency.

We present direct numerical simulation results for a large number of realizations of the quenching problem in figure 5. For this exploration, (1) with (12) is solved on an interval of $0 \leq t \leq L/(2\hat{\epsilon})$ with an $N = 1 + 2^{13}$ point spatial discretization and $O(h^{12})$ centered-difference approximation of the diffusion operator, where $h = L/(N - 1)$, using CVODE in the Sundials package [24–26] with a matrix-free GMRES solver for the linear system. These numerical parameters reproduce the constant $\psi(t)$ for a stable pulse over the $T = L/(2\hat{\epsilon})$ interval to a tolerance of $|\psi(T) - \psi(0)| < 10^{-5}$. For these large finite-difference approximations, we focus on the root-finding problem over a bounded region of the (x_s, θ) -plane.

Figure 5 shows the DNS results of the quenching problem for the stable pulses shown in figure 3. Note that the perturbation width is positively-valued, and perturbations with unresolvable widths, i.e. $x_s < 2L/N$, are restricted. The perturbation parameter θ is chosen to position the perturbation behind ($\theta < 0$) or ahead ($\theta > 0$) of the peak for the stable pulse. The color designates the solution to (11): either a solution to the bisection problem is found (oranges) or *no solution* (blue) is found for $U_q \in [-10^3, 0)$. A narrow gap (white) between the successful and unsuccessful regions exists as the triangulation for both regions is conservative. While it is possible that $U_q \rightarrow -\infty$ in the white region, we expect that actually the finite cutoff is real in the sense that the largest amplitude for a successful quenching is substantially smaller than the root-finding limit. That is, if we expect that U_q diverges for some (x_s, θ) , then we should find saturation of $U_q \approx -10^{+3}$ near the bounds of the effective quenching regions. We do not observe this in the data, as $|U_q| \ll 2 \times 10^{+2}$, across the entire range of γ , and $|U_q| < 10^{+1}$ for $\gamma = 0.001$.

The successful quenching parameters are bounded in the (x_s, θ) -plane by lines with slope approximately $\pm 1/2$, which intersect at (x_s^0, θ^0) coordinates which correspond to the quenching perturbation with minimal width and corresponding optimal position. We compute the slopes and intercepts using an exterior penalty method and find the deviation in the discriminator slopes from $\pm 1/2$ is $< 5 \times 10^{-3}$. For sufficiently small time-scale separation parameter, $\gamma < 0.02$, we find that the minimal width is finite, corresponding to $x_s^0 \approx 79$ and $x_s^0 \approx 2$ for $\gamma = 0.001$ and $\gamma = 0.010$, respectively, cf. figure 6(a,b). For $\gamma \geq 0.020$, we find that the linear bounding estimate for the minimum quenching width vanishes; i.e. the linear bounds of the successful quenching parameters intersect at $x_s^0 < 0$. The successful quenching numerics fall short of resolving infinitesimally thin perturbations, bounded from below by the grid spacing $L/(N - 1) \approx 0.33$, but they confirm this bound up to the discretization limit, cf. figure 6(c,d). The reproduction of the limited region

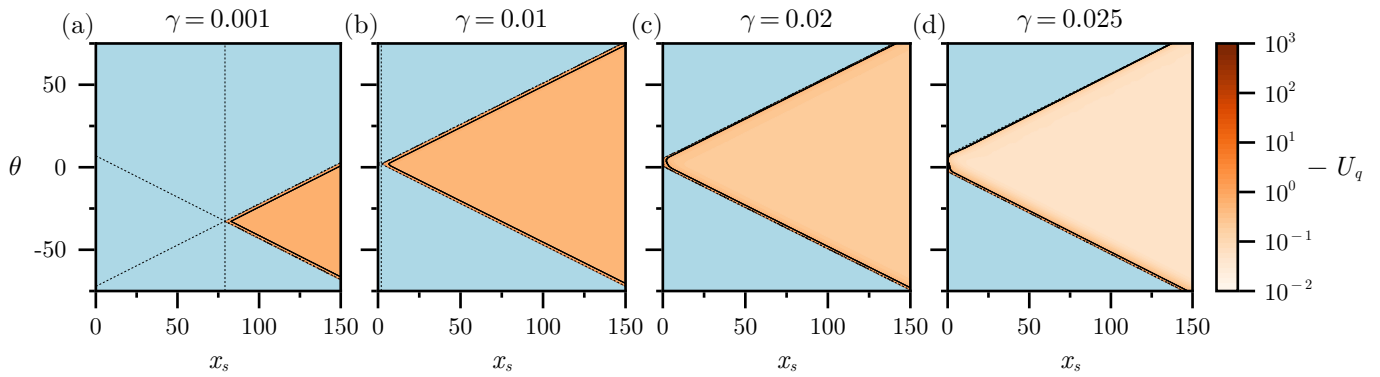


FIG. 5. Critical quenching perturbations sampled over the (x_s, θ) -plane, for (a) $\gamma = 0.001$, (b) $\gamma = 0.010$, (c) $\gamma = 0.020$, and (d) $\gamma = 0.025$. In all cases, the perturbation quenching amplitude U_q determines the red color and blue denotes regions in which (11) has no solution for all bounding samples (c.f. black dots in figure 6(a-d)). The $|\beta - 1|$ asymptotic estimate contour is denoted by a solid black curve and the linear bounding region between successful and unsuccessful quenching searches is denoted by black dashed lines.

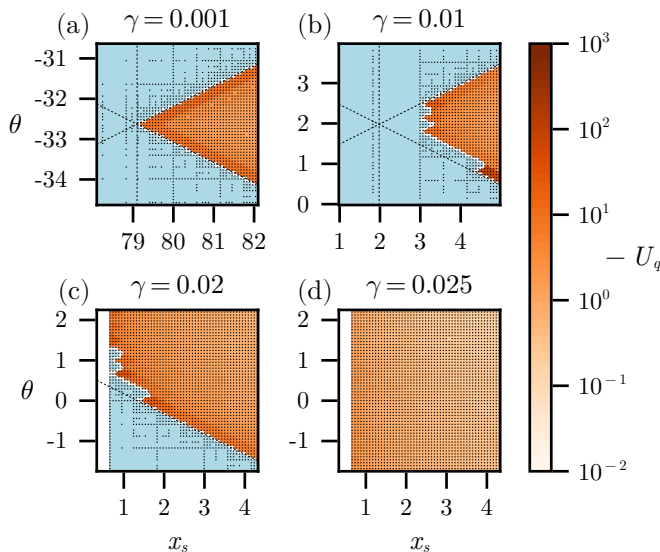


FIG. 6. Critical quenching perturbations near the smallest quenching perturbation width for $\gamma \in \{0.001, 0.01, 0.02, 0.025\}$ in (a-d), respectively. Colors are as in figure 5(a-d), with black dots representing sampled quenching parameters.

of quenching possibility is thus an important test for the predictive quenching theory presented in this work.

Predictions of the critical quenching amplitude (color dashes) and DNS results (black \circ) are compared in figure 7, for $\theta \in \{-10, -5, 0, 5, 10\}$, and for $x_s \in [2L/N, L/2]$. The linear theory predictions agree with the DNS results across one or more decades of x_s , for some values of θ , for most choices of l and γ . The prediction is most effective when the stable and unstable pulses are close in shape, as the $\gamma = 0.025$ quenching amplitudes are reliably predicted across a wider range of θ , x_s , and $U(s; \theta, x_s)$ than for $\gamma = 0.020$, as explained in the theory construction. For $\gamma = 0.025$, perturbations centered at or

immediately ahead of the peak of the stable pulse ($\theta \geq 0$) are able to quench the excitation for smaller perturbation widths and smaller amplitudes, while perturbations centered behind the peak of the pulse ($\theta < 0$) are successful over a smaller range of perturbation widths and the rate at which the critical quenching amplitude grows is significantly faster, c.f. (d) and (t). This is expected—as a narrow perturbation appears at $\theta > 0$ and $t = 0$, the stable pulse effectively runs into the perturbation by time $(\theta - x_s/2)/\check{c} \ll L/2\check{c}$, which drives the dynamics away from the stable solution. Meanwhile, for narrow perturbations which are centered behind the peak of the wave, only the main excited region and tail of the stable pulse are affected—in this sense it is the front which controls the effectiveness of quenching perturbations. The intuition that front recovery in FitzHugh-Nagumo models is robust thus appears correct, at least for sufficiently small γ or large time-scale separation; this important feature is not reflected in the predicted quenching amplitudes, which are approximately invariant with respect to perturbation width to much smaller x_s .

The separation between the slow and fast wave morphology impacts the asymptotic critical amplitude. This is easiest to see for $\gamma = 0.001$, where the steep wave front and wave back of the stable pulse lend itself to a rectilinear approximation. The stable pulse $\check{u}_1(x)$ crosses zero at $x \approx x_a$ and $x \approx x_b$, and $0.8 \lesssim \check{u}_1(x) \lesssim 1$ in the excited region. This indicates that for $\theta \approx (x_a + x_b)/2$ and $x_s \gtrsim |x_b - x_a|$, all quenching perturbations should succeed with $U(s; \theta, x_s) \gtrsim \beta - 1$ (the maximal distance between the unstable and excited $f_1 = 0$ nullclines). In figure 7(a,e,i,m,q), the critical quenching amplitude has $|U(s; \theta, x_s)| \approx 0.8$ which is comparable to $1 - \beta \approx 0.86$. Likewise, figure 5(a) shows there is little variation in the value of $|U_q|$ within the successful region, and that the region is approximately bounded by $|\beta - 1|$. Unexpectedly, the critical amplitude varies with the timescale separation parameter γ , as β is held consistent throughout. This indicates that our expectation from the asymptotic

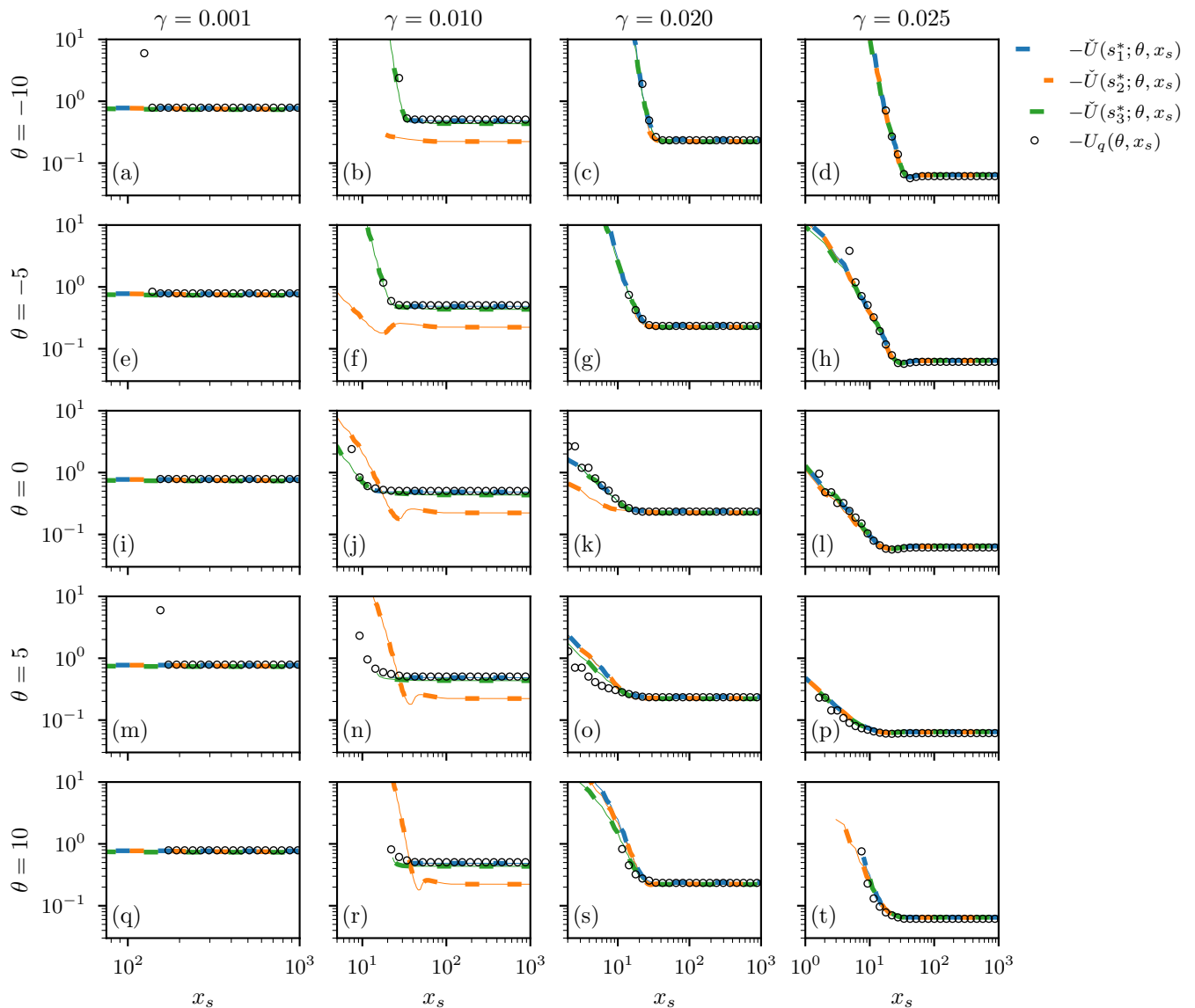


FIG. 7. Critical quenching predictions for the FitzHugh-Nagumo model (color) using selectors $\tilde{\mu}_1$ (blue), $\tilde{\mu}_2$ (orange), and $\tilde{\mu}_3$ (green), and quenching computed using DNS of the perturbed stable pulse (black, \circ).

solution, $U_q \rightarrow \beta - 1$, is not relevant for time-scale separations as small as $\gamma \gtrsim 0.01$. While $\gamma = 0.01$ corresponds to a bifurcation for the stable rest state, which we do not anticipate to be relevant for the quenching problem.

B. Mitchell-Schaeffer model

The Mitchell-Schaeffer model [27] is a simplified model of cardiac cell excitation, combining two state components to produce a realistic description of action potential shape and restitution. It is derived from an asymptotic reduction of the Fenton-Karma model [28] of atrial excitation by the adiabatic elimination of the fastest processes. The Mitchell-Schaeffer model preserves multiple decay timescales, which we recombine to form an explicit

time-scale separation and slow-fast system,

$$\begin{aligned} f_1 &= u_1^2(1 - u_1)u_2 - u_1\tau_i/\tau_u, \\ f_2 &= \varepsilon((1 - u_2)H_k(u_g - u_1)\tau_c/\tau_o - u_2H_k(u - u_g)), \end{aligned} \quad (13)$$

where we have introduced $H_k(x) = (1 + \tanh(kx))/2$. The standard parameter values are $\tau_i = 0.3$ ms, $\tau_o = 120$ ms, $\tau_u = 6$ ms, $\tau_c = 150$ ms, $u_g = 0.03$, and $k = 100$. We keep $\tau_i/\tau_u = 0.05$ and $\tau_c/\tau_o = 1.25$ fixed, while allowing the non-dimensional ratio of the longest and shortest time-scales, ε , to vary.

Additionally, we have treated the Mitchell-Schaeffer model differently from the FitzHugh-Nagumo model and considered *pulse train* solutions of the model instead of *homoclinic* solutions. This ultimately assesses the ability of the linear theory to predict quenching perturbations for pulses which are not isolated, i.e. in analogy to

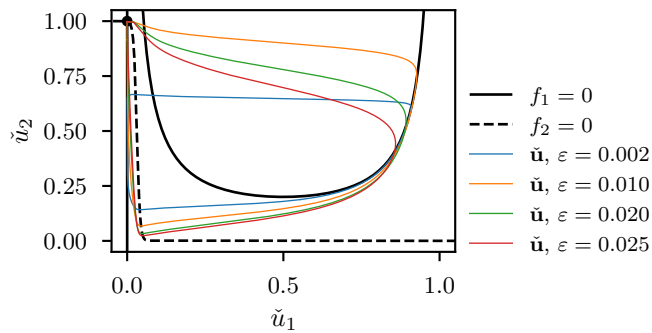


FIG. 8. Nullclines of the Mitchell-Schaeffer model ($f_1 = 0$ black, solid; $f_2 = 0$ black, dashed) and the stable pulse train solutions for $L = 500$ for $\varepsilon \in \{0.002, 0.01, 0.02, 0.025\}$.

tachycardia-like scenarios. Figure 8 shows the nullclines of the model with the stable pulse train solutions on a ring of length $L = 500$, for $\varepsilon \in \{0.002, 0.01, 0.02, 0.025\}$. We choose $\varepsilon \geq \tau_i/\tau_c$ to improve the stiffness of the model while permitting the study of quenching for fast solutions which are close, in an L^2 -sense, to their slow counterparts. All states and eigenfunctions are posed on a periodic domain of length $L = 500$, so that for $\varepsilon > 0.01$ the stable wave is effectively isolated, while for $\varepsilon = 0.002$ the stable pulse train does not relax to the quiescent state (the unstable wave is isolated for all ε considered).

Figure 9 shows the linear theory ingredients for the Mitchell-Schaeffer model. Surprisingly, the scaling of the leading eigenfunctions is still affected by the variation in

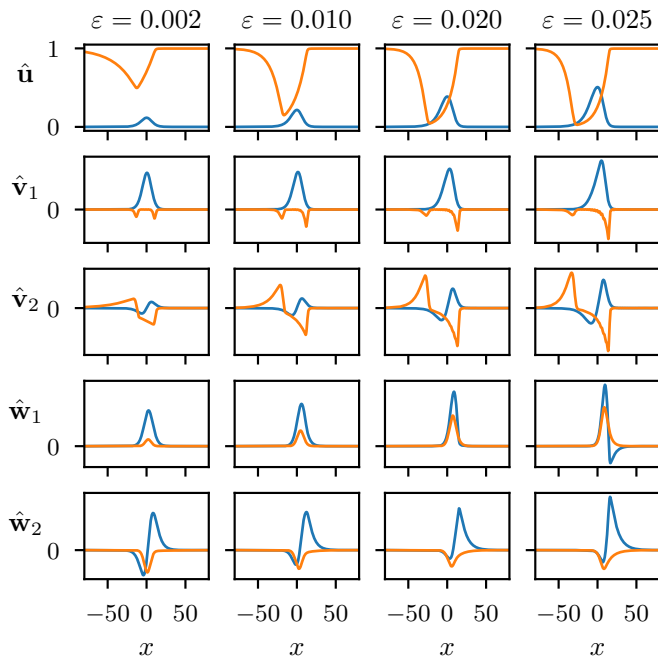


FIG. 9. Linear theory ingredients for the Mitchell-Schaeffer model. (Top row) Unstable pulse solution $\hat{\mathbf{u}}$ for $\varepsilon \in \{0.002, 0.010, 0.020, 0.025\}$, with (second row) $\hat{\mathbf{v}}_1$, (third row) $\hat{\mathbf{v}}_2$, (fourth row) $\hat{\mathbf{w}}_1$, and (fifth row) $\hat{\mathbf{w}}_2$.

ε by $O(10^1)$ – such that, for $\varepsilon = 0.002$, similar considerations about the predictive power of the method should be taken into account relative to $\varepsilon = 0.025$. We supply the linear theory ingredients to the prediction program to estimate the necessary quenching amplitude for a variety of perturbation widths and positions.

The critical quenching predictions for the Mitchell-Schaeffer model are shown in figure 10 for $\theta \in \{-10, -5, 0, 5, 10\}$. The critical quenching predictions are quite similar to those produced by the FitzHugh-Nagumo model, despite the very different structures of the models – Mitchell-Schaeffer is an ionic model, while FitzHugh-Nagumo is not. Both predictions transition from quasi-constant regions of perturbation amplitude when x_s is large to quickly growing critical quenching amplitude for smaller widths. The sensitivity to the position of the perturbation is more subtle in the Mitchell-Schaeffer model, i.e. we do not see substantial variation in the lower bound of x_s across θ , and the sensitivity to the difference between the fast and slow waves (i.e., ε) is more severe. In particular, for small time-scale separation ($\varepsilon = 0.025$) we observe a finite (soft) lower bound for x_s in both the DNS and linear predictions, distinct from FitzHugh-Nagumo. Likewise, the transition to growing quenching amplitudes for small x_s is rarely relevant; instead nearly every prediction is within a tight tolerance of the asymptotic prediction, and the DNS quenching results only show growing quenching amplitudes for very small regions of the (x_s, θ) -plane.

It is for the more similar pairs of waves (e.g., $\varepsilon = 0.025$) that the difference between the heuristics is most clear, especially in the asymptotic $x_s \rightarrow \infty$ regime. The predictions for large x_s are only accurate for $\check{\mu}_3(s; \theta, x_s)$; while $\check{\mu}_2(s; \theta, x_s)$ systematically under-estimates the magnitude of the perturbation, and $\check{\mu}_1(s; \theta, x_s)$ over-estimates the quenching amplitude specifically for large x_s . Of particular note is that for $\varepsilon \geq 0.020$, the transition from the asymptotic regime to larger quenching amplitudes is effectively captured by the linear theory (using $\check{\mu}_3(s; \theta, x_s)$), such that the linear theory may accurately predict quenching applied solely to the wavefront, an essentially nonlinear effect. The success of determining the transition length indicates that the linear prediction theory would benefit significantly from a consideration of higher-order effects, such that the applicability of the theory to larger time-scale separations could capture the linear-to-nonlinear transition for quenching, and predict successful the quenching of the wavefront for ionic models.

V. DISCUSSION

Some combinations of heuristic and parameters leads to considerably less accurate predictions; notably $\check{\mu}_2(s; \theta, x_s)$ for $\gamma = 0.01$ in figure 7, where the prediction for the critical quenching amplitude differs by a factor of roughly 10 compared to $\check{\mu}_{1,3}(s; \theta, x_s)$. Consider

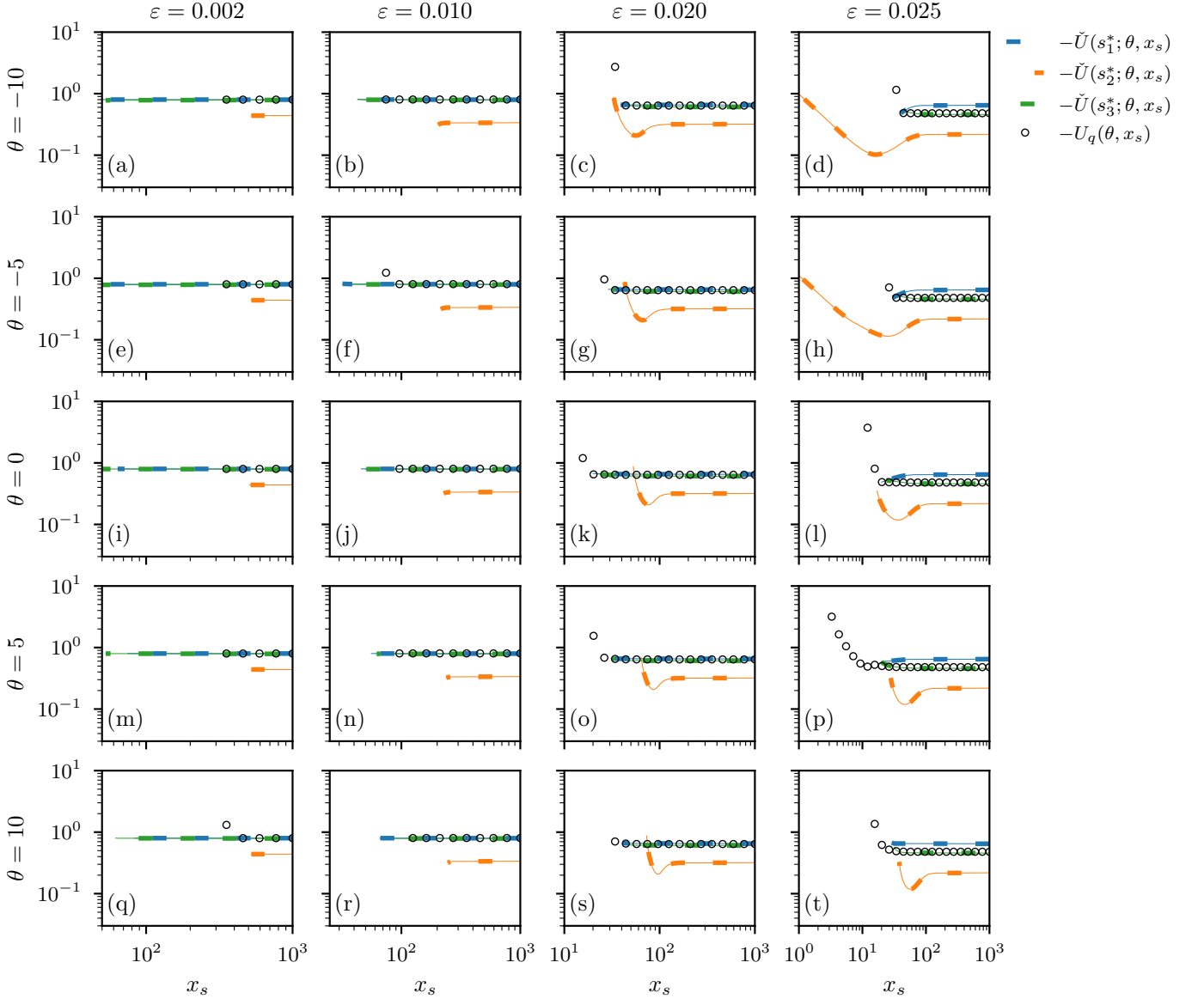


FIG. 10. Critical quenching amplitude predictions using $\check{\mu}_1(s; \theta, x_s)$ (blue), $\check{\mu}_2(s; \theta, x_s)$ (orange), and $\check{\mu}_3(s; \theta, x_s)$ (green) compared to the quenching amplitude computed using DNS of the perturbed stable pulse (black, \circ).

the similarity of $\check{\Phi}_2(x-s; s)$ and $\check{\Phi}_3(x-s; s)$; i.e. the two correspond precisely for self-adjoint problems where $\hat{\mathbf{w}}_j \equiv \hat{\mathbf{v}}_j$. With no further effort we may confidently blame the non-normality of the critical wave linearization and concomitant scaling of the components of the unstable pulse and eigenfunctions. [16] We seek the dominant contribution to $\check{\mu}_2(s; \theta, x_s) - \check{\mu}_3(s; \theta, x_s)$ in the neighborhood of $s = s_3^* : \check{\mu}_3(s_3^*; \theta, x_s) = 0$. As the perturbation envelope is unaffected by the details of this expansion,

we consider the $\check{\Phi}_l(x-s; s)$ directly,

$$\begin{aligned} & \check{\Phi}_2(x-s; s) - \check{\Phi}_3(x-s; s) \\ &= \check{\Phi}_2(x-s_3^* - \delta; s_3^* + \delta) - \check{\Phi}_3(x-s_3^* - \delta; s_3^* + \delta), \\ &\approx \check{\Phi}_2(x-s_3^*; s_3^*) \\ &+ \delta \cdot \partial_s (\check{\Phi}_2(x-s; s) - \check{\Phi}_2(x-s; s)) \big|_{s=s_3^*} + O(\delta^2). \end{aligned}$$

We elect to consider the $O(\delta)$ term directly, dropping the implicit dependence of the unstable pulse and eigenfunctions on $\xi = x-s$, and simplifying

$$\begin{aligned} & \delta^{-1} (\check{\Phi}_2(x-s; s) - \check{\Phi}_3(x-s; s) - \check{\Phi}_2(x-s_3^*; s_3^*)) \\ &= \langle \hat{\mathbf{v}}_2 | \hat{\mathbf{u}} - \check{\mathbf{u}}(\xi + s_3^*) \rangle \hat{\mathbf{w}}_1 \\ &+ \langle \hat{\mathbf{w}}_2 - \hat{\mathbf{v}}_2 | \hat{\mathbf{u}} - \check{\mathbf{u}}(\xi + s_3^*) \rangle \partial_x \hat{\mathbf{w}}_1 \\ &+ \langle \hat{\mathbf{w}}_1 | \hat{\mathbf{u}} - \check{\mathbf{u}}(\xi + s_3^*) \rangle \partial_x (\hat{\mathbf{w}}_2 - \hat{\mathbf{v}}_2). \end{aligned} \tag{14}$$

Since we are interested in the perturbation magnitude in the asymptotic limit, we take $\delta \equiv s_2^* - s_3^*$ and take the inner product with $\check{\mathbf{X}}(x - \theta; x_s)$ with (14) and take $\lim_{x_s \rightarrow \infty}$,

$$\begin{aligned} \lim_{x_s \rightarrow \infty} \delta^{-1} (-\check{\mu}_3(s_2^*; \theta, x_s) - \check{\mu}_2(s_3^*; \theta, x_s)) \\ = \langle \hat{\mathbf{v}}_2 | \hat{\mathbf{u}} - \check{\mathbf{u}}(\xi + s_3^*) \rangle \langle \hat{\mathbf{w}}_1 | \check{\mathbf{X}}(x - \theta; x_s) \rangle. \end{aligned} \quad (15)$$

That is, in the asymptotic limit the inner products with differentials of the eigenfunctions become the eigenfunctions evaluated at their endpoints which are equal for the pulse solutions, leaving only the term proportional to $\hat{\mathbf{w}}_1$. We estimate the magnitude of δ by inverting (15),

$$\delta \approx - \frac{\check{\mu}_3(s_2^*; \theta, x_s) + \check{\mu}_2(s_3^*; \theta, x_s)}{\langle \hat{\mathbf{v}}_2 | \hat{\mathbf{u}} - \check{\mathbf{u}}(\xi + s_3^*) \rangle \langle \hat{\mathbf{w}}_1 | \check{\mathbf{X}}(x - \theta; x_s) \rangle},$$

and note that generically the numerator will be small (but typically non-zero), while the denominator will be large. If we assume that $\partial_s U(s_3^*) = 0$ (i.e., $\check{\mu}_3(s; \theta, x_s)$ extremizes the perturbation amplitude), then

$$|U(s_2^*) - U(s_3^*)| \approx \frac{\delta^2}{2} |\partial_s^2 U(s_3^*)|, \quad (16)$$

which may be $O(|U(s_3^*)|)$, even if δ is small (cf. Appendix 2 for numerical details).

Finally, we return to the question of how to best measure the inter-state distance for the selection of an appropriate frame; i.e. how should we construct $\check{\mu}_l(s; \theta, x_s)$ using the ingredients of the stable and unstable state for the purposes of predicting quenching? In contrast to the ignition case, for quenching we can make a strong argument for the third heuristic, which chooses a frame in which the projection onto the center-stable eigenmode of the unstable pulse is identically zero. It is simple to see that, if the L^2 -distance is already small—when the fast and slow pulses are similarly shaped—then $\check{\mu}_3$ determines a frame which is close to the one in which the perturbation does not excite the translational mode of the *stable* wave in addition to the unstable wave. In this way, the perturbation generated from the third heuristic may be seen as more efficient for quenching. However, the numerical evidence suggests that no single frame selector is uniquely prescient—for FitzHugh-Nagumo and $\gamma > 0.01$, all three predictors give nearly indistinguishable results for all cases; while for $\gamma = 0.01$, $\check{\mu}_2(s; \theta, x_s)$ is uniquely poor. For $\gamma = 0.001$, no heuristic accurately captures the lower bound of x_s for effective quenching observed in the DNS. This suggests a different criterion by which to consider the frame selectors: *which produces the fewest wrong (especially smaller-amplitude) predictions in the parameter ranges over which DNS results show that quenching is possible?* For FitzHugh-Nagumo with $\gamma = 0.010$, $\check{\mu}_2(s; \theta, x_s)$ is unambiguously worst by this metric, as it systematically underestimates the quenching amplitude. To put such predictions into practice would fail to halt an excitation—which in a medical context could be disastrous.

VI. CONCLUSIONS

Given a stable propagating solution and a family of perturbations parameterized by their width x_s and position θ , we are able to predict the critical quenching amplitude which corresponds to the cessation of propagation. The method is effective in the archetypal FitzHugh-Nagumo model with isolated pulse solutions and the Mitchell-Schaeffer model with pulse train solutions. We find that the linear theory achieves qualitative accuracy with minimal insight, and quantitative accuracy in regimes where the linear assumptions of the perturbation theory are valid and the leading adjoint eigenfunctions are ‘small’ in a sense preserved by the norm. The method is sufficiently fast and parsimonious to be useful in optimization searches, and thus opens new avenues for the selection of *optimal* positions θ and widths x_s in addition to the prediction of the critical amplitude for such pairings. Finally, we find the predominant shortcoming of the application of the linear theory is the determination of the *correct* reference frame, as no generally applicable uniqueness results are available, though in practice we may resolve such difficulties through continuation. We expect that additional heuristics, in analogy with the critical ignition problem, may be reasonably considered, but have focused primarily on the numerical results in this work.

A similar quenching effect was investigated numerically in the modified three-component Oregonator, and experimentally using optical control methods in the Belousov-Zhabotinskii reaction. [29] That work considered specifically time-distributed controls in the co-moving frame of the pulse, i.e. those of form $\check{\mathbf{X}}'(x - \theta - \check{c}t; x_s)\Theta(t)$, which differs from those investigated in this work $\check{\mathbf{X}}(x - \theta; x_s)\delta(t)$. Nonetheless, in that work their ‘dev’ is analogous to our θ , their d_{irrad} is analogous to our x_s , and their $\varepsilon_{\text{irrad}}$ is analogous to our $|U_q|$. An extension of the present theory to co-moving perturbations requires the integration of accumulated differences in the state from the stable wave, which we leave for a future application.

We have not treated the construction of optimal perturbations in this manuscript, in either the linear [30] nor the nonlinear [31] cases. Likewise, we have not considered the more general case of optimal control of cardiac excitation patterns using, e.g., adjoint flow optimization of a stimulating current or applied electric field [32]. As the spectrum of the stable solution is, in all cases, $\text{Re}(\sigma) \leq 0$, the correspondence between the linear prediction, transient amplification due to the non-normality of the Jacobian, and the direct numerical simulation of an optimally constructed perturbation presents a uniquely novel verification for the method presented. However, the optimal perturbation construction requires a significant number of eigenmodes for the successful prediction of the transient amplification (i.e. it relies on the formation of $O(N^2)$ products $\langle \check{\mathbf{v}}_i(t) | \check{\mathbf{v}}_j(t) \rangle$ at times $t = 0$ and the optimization time) [33], while the nonlinear optimal perturbation requires adjoint flow optimization [34]. For

the stable waves in this study typically only a few leading eigenmodes are readily computed due to the stiffness of the underlying discretized system, and none are used in the calculation. In this light, the parsimony and computational efficiency of the presented linear theory is an asset for quenching predictions.

An extension of the current approach to account for front solutions—solutions $\tilde{\mathbf{u}}$ of (2) where $\lim_{x \rightarrow +\infty} \tilde{\mathbf{u}}(x) \neq \lim_{x \rightarrow -\infty} \tilde{\mathbf{u}}(x)$ —is ongoing. Our asymptotic arguments rely on the far-field properties of the eigenfunctions and state for convergence; since front solutions should also have reasonably localized leading eigenfunctions, only the latter presents an issue for the theory. Fast algorithms for the computation of the Fourier extension are known with strong guarantees of convergence [35], and the application of such techniques to front solutions and their eigenfunctions would enable us to treat the inputs similarly to the pulses for the numerical application of the theory. Initial explorations report multiple frames for effective quenching related by a symmetry $\tilde{\mu}_\ell(s^*) = \tilde{\mu}_\ell(s^* + L)$, which we filter based on the original domain length, but the predictions of the critical quenching amplitude are inaccurate for some configurations of perturbation and model.

We have not addressed the possibility that some optimal heuristic that determines the frame s for each (x_s, θ) pair absolutely uniquely may be constructed, whether by analytical insight or numerical effort. The latter, we expect, should take the perturbation parameters determined accurately by DNS, (x_s, θ, U_q) , and use these to find appropriately parsimonious combinations of the leading eigenfunctions and solutions, analogously to SINDy methods. [36] Building a kriging model at runtime which maps (x_s, θ, U_q) triplets to $s : U(s; \theta, x_s) = U_q$ may be a good use for other machine learning techniques, where the universal approximation capabilities of sufficiently large neural networks may be of use. [37] Indeed, one may train a neural network of sufficient complexity to predict the critical excitation amplitudes from the (x_s, θ, U_q) tuples, directly. A downside to the machine learning approach is the loss of interpretability—the existing heuristics all follow from fairly simple considerations of the critical solution eigenmodes and linear theory. Preliminary experiments indicate that simple neural network approximations of the critical quenching amplitude are specific to the particular excitable model and parameter set, and thus the data generation processes lack sufficient generality. Likewise, forming the critical quenching training dataset is either too computationally demanding (so that applying a neural network does not represent a significant computational savings) or is too small for a trained neural network to estimate the probability of success near the quenching boundary (so such predictions are not robust). The notion of a reference frame, and the deviation from initial to final states may prove too restrictive to generate generalizable, interpretable, and predictive machine learning models for the quenching amplitude at this stage.

A significant hurdle for the application of the present theory to physical systems is the question of medium or tissue heterogeneity. Without a homogeneous medium, the selection of the reference frame loses meaning; in what sense can the shift be selected if the system no longer exhibits the relevant symmetry? The systems to which we may seek to apply this theory exhibit significantly less sensitivity to perturbations far from the salient features of the state; in the one-dimensional context this is the critical wave peak, and in higher dimensions this is a topological feature of the state (i.e. spiral origins or scroll wave filaments) [38–40]. Similar considerations for the sensitivity of spiral waves to localized medium heterogeneity [39, 41, 42] suggest this hurdle can be overcome—and in the extreme case where the heterogeneity affects the critical wave peak, may only affect the confidence in predictions for the critical quenching amplitude locally. Likewise, the linear theory may be extended for such heterogeneous media by treating “small” deviations from homogeneity as perturbations analogous to the quenching perturbation; this approach will be considered rigorously in future work.

VII. ACKNOWLEDGEMENTS

CDM would like to thank Prof. Vadim Biktashev (University of Exeter) for helpful discussions.

APPENDIX

1. Traveling wave continuation & eigenproblems

As mentioned in the main text, we compute families of excitation pulses using AUTO-07P [19]. This involves casting (1) into first-order form in u_1 , u_2 , and $u_3 \equiv \partial_x u_1$:

$$\begin{aligned} u'_1 &= u_3, \\ u'_2 &= -f_2(u_1, u_2)/c, \\ u'_3 &= -(cu_3 + f_1(u_1, u_2) + J)/D, \end{aligned} \tag{17}$$

where $c > 0$ and $D > 0$. An initial condition corresponding to the quiescent state, $\bar{\mathbf{u}}$, appended with an extra zero corresponding to the first derivative of \bar{u}_1 , serves as initial condition. The system is then continued in the stimulation current J to a Hopf bifurcation, at which point the solver switches to the family of periodic orbits emanating from the bifurcation, now in (J, c) . When states of sufficient length are found, the periodic solutions are continued until $J = 0$, and the resulting solution serves as a starting point for the continuation to generate an interesting family of solutions; e.g., for FitzHugh-Nagumo, in (γ, c) as depicted in figure 3. In the experiments presented in this work, we use $\text{NTST} = 1000$ and $\text{NCOL} = 4$, leading to a 4001-element discretization of the pulse at each (γ, c) -pair. The solutions generated by this process are then written to file, along with their parameters.

We use the AUTO-07P generated solutions as initial estimates for a boundary value problem (BVP) posed on a Chebyshev domain with M basis modes, and $N = 2M$ grid points; when $N > M$, the calculation of nonlinear terms is more accurate due to dealiasing of the underlying nodal integrals. The boundary value problem (BVP) is constructed in DEDALUS2 [20], and the same system is used for the eigenvalue (EVP) and initial-value problems (IVP). As DEDALUS2 requires casting the system to first order in Chebyshev-basis spatial derivatives, we arrive at system (17); as a third order system in two (primary) variables, in order to avoid asymmetric boundary conditions (which will, typically, pollute the eigenspectrum of the pulse) [43, 44]. We shall also note that the implementation in DEDALUS2 uses an implicit Tau method, which is equivalent to dropping the rows in the discretization corresponding to the highest frequency modes in the Chebyshev expansion and replacing those rows with the boundary conditions. Thus our BVP, EVP, and IVP solutions are technically only correct to the leading $M-3$ modes. More general tau methods are available in DEDALUS3 through explicit inclusion of tau terms [45].

The boundary conditions used in the solution of this BVP are projective [16], which permits the finite expansion to approximate the homoclinic orbit rather than the periodic wave train solution (which would be used with the periodic boundary conditions of the AUTO-07P periodic orbits). We refine the solution on the dealiasing Chebyshev grid using a Newton solver for the system until the maximum of the Newton updates is smaller than 5×10^{-15} and the Newton update contains all the energy in the dealiasing modes (i.e., modes larger than M). For the FitzHugh-Nagumo model, $M = 2^{12}$, which we found to be sufficient on a domain of size $L = 2700$. Likewise, as the domain is significantly larger than the critical pulse, the projective boundary conditions effectively satisfy periodic boundary conditions up to an error in the deviation of the endpoints from the rest state; in our experience, this is smaller than 10^{-13} , but there is no known guarantee for the exactness of this approximation for the Chebyshev-T expansion on Gauss-Quadrature nodes.

The refined BVP solution is then passed to an EVP solver, which constructs the linearized system about the solution using (analytical) expressions for $f_{ijk} \equiv \partial_i \partial_j f_k$, $i, j, k \in \{1, 2\}$:

$$\begin{aligned} 0 &= \sigma v_1 - (Dv'_3 + cv_3 + f_{101}v_1 + f_{011}v_2), \\ 0 &= \sigma v_2 - (cv_3 + f_{102}v_1 + f_{012}v_2), \\ 0 &= v_3 - v'_1, \end{aligned} \quad (18)$$

for the eigenvalue σ , on the same Chebyshev domain as was used in the BVP (with the datatype elevated to `complex128`, to account for complex-valued modes). The EVP solver likewise inherits the projective boundary conditions from the BVP solver. However, the EVP solver may be used to compute the left or right eigenmodes by appropriate substitutions in the formation of the eigenproblem, especially the boundary conditions.

Finally, we consider the IVP used in the direct numerical simulation of perturbed stable waves. Since we already have a preponderance of solutions computed using a finite-difference method and adaptive time-stepping, we treat the spectral solution of the IVP as a verification of the results. This calculation reuses the same the M -mode solutions of the BVP solver to form the initial condition. In general, one should treat the extension from the BVP solution with projective boundary conditions to the IVP with periodic boundary conditions basis carefully. The former is a segment of the infinitely long homoclinic orbit solution, while the latter is a periodic orbit “close” to the homoclinic for sufficiently large L , M , and N . In practice, we treat the extension as both a check that we have sufficiently resolved the tails of the solution in the homoclinic case (by comparing the difference in the state variables at the endpoints), and an effective limit to our solution accuracy for the periodic problem. The initial condition is then perturbed according to the perturbation bisection problem detailed in the text, which makes the initial condition non-smooth; for this reason we do not dealias the state for the IVP ($N = M$) to account for the sharp features of the perturbations to the state for the quenching problem. Given the non-smooth initial condition, we found it was necessary to make small timesteps initially, which we manage by multiplying the base time step by a power of 2 based on the progress of the simulation. That is, at time $0 \leq t_i \leq T$, $t_{i+1} - t_i = \min([\max([\log_2(t_i/T + 2^{-12})], -12]), 0) \times \delta t$; so initially, the simulation makes 2^{12} times more time-steps per unit time than at the end of the simulation. This stabilizes the already strongly dissipative SBDF4 method [46] when $U(s, \theta)$ is large, i.e., $\sim -10^2$). The root-finding problem for the amplitude is solved to a tolerance of 10^{-10} for each (x_s, θ) pair by repeatedly calling the IVP with perturbed initial conditions within a bisection procedure, with early exit in the case that $\|\mathbf{u}(t, x) - \bar{\mathbf{u}}\|_1 < 10^{-10}$ and $t < T = L/(2\tilde{c})$.

2. Root-finding and continuation

As the determination of the optimal frame is posed in terms of a scalar root-finding problem, cf. (8), and $\tilde{\mu}_l(s; \theta, x_s)$ is generally an unknown but very complicated function, significant care in the identification, refinement, and interpretation of roots must be taken. Of particular relevance for the predictions of the linear theory, we have no strong guarantees of uniqueness for the roots of $\tilde{\mu}_l(s; \theta, x_s)$ for any every given perturbation envelop $\check{\mathbf{X}}(x - \theta; x_s)$, nor for any model-supplied $\hat{\mathbf{u}}(\xi)$, $\hat{\mathbf{w}}_2(\xi)$, and $\hat{\mathbf{u}}(\xi + s)$.

As part of the published linear theory code [18], we construct $\tilde{\mu}_l(s; \theta, x_s)$ two ways: using the convolution approach detailed in the main text, and through explicit reconstruction and shifting of $\Phi_l(x - s)$ to form

$$\tilde{\mu}_l^1(s; \theta, x_s) \equiv \langle \Phi_l(x - s) | \check{\mathbf{X}}(x - \theta; x_s) \rangle \quad (19)$$

for a significant number of test shifts $s \sim U[0, L]$. Deviations are on the order of $|\check{\mu}_l(s; \theta, x_s) - \check{\mu}_l^1(s; \theta, x_s)| \sim 10^{-10} - 10^{-6}$ for the problems considered, which is sufficient for the linear theory predictions; we note the maximum error as `tol` such that $1 \gg \text{tol} > 0$.

Indeed, the leading issue with the direct application of the linear theory (instead of the continuation from asymptotic regimes) is not the inaccuracy of scalar root-finding (this would imply that the optimal frame is adjacent to extremely sub-optimal frames), but rather from the often extremely large number of roots initially computed resulting from oscillations in the input fields. The linear prediction code interpolates the input fields onto a Fourier grid of fixed size to speed up the convolutions; typically 2^{13} is sufficient for our purposes, as the number of grid points only affects the resolution of the predictions for very small perturbation widths. However, the Fourier expansion guarantees that the number of roots of $\check{\mu}_l(s; \theta, x_s) = 0$ is an even number. For the 2^{13} Fourier expansion, we will typically find between 2 and 2×10^3 prospective roots without additional insight; thus the uniqueness of the asymptotic perturbation is essential for tractability.

Unfortunately, the continuation requires the solution of all intermediate problems for small perturbation widths, which may be prohibitive in some circumstances, and is inefficient compared to a direct computation for any single x_s . In principle, the direct computation may compute the correct asymptotic branch, but does not determine it uniquely; it is unclear whether a filtering process applied to the roots specifically may discriminate the asymptotic branch without computing the asymptotic solution. For numerical reasons, the direct (non-continuation) calculation requires the introduction of filters based on the value of `tol` determined by the comparison of $\langle \Phi_l(x-s) | \check{\mathbf{X}}(x-\theta) \rangle$ and $\check{\mu}_l(s; \theta, x_s)$, c.f. discussion surrounding (19). The filters introduced for the direct computation are,

1. The first filter considers only isolated roots – if s^* denotes the set of proposed roots, we consider only those where where $|\check{\mu}_l'(s^*)| > \text{tol}$. This is typically the most significant filter, as it removes large swaths of roots which correspond to high-frequency, low-amplitude, oscillations about zero. In extreme cases, a reduction from $O(10^3)$ to $O(10^1)$ potential roots.
2. The second filter considers only those roots where the leading adjoint eigenmode has a non-trivial projection onto the perturbation – $|\langle \hat{\mathbf{w}}_1(x-s^*) | \check{\mathbf{X}}(x-\theta; x_s) \rangle| > \text{tol}$.
3. At this stage many roots persist and their quenching amplitude predictions may be made almost arbitrarily large if the denominator of (6) is suffi-

ciently small, which is addressed in the prior filter. The final filter rejects proposed frames for which the projection of the perturbation onto the leading eigenfunction is significantly smaller than the projection of the stable state, i.e. s^* for which $|U(s^*, \theta)| < \text{tol}^{-1}$.

The application of the above filters will still leave several proposed roots s^* , and often distinct roots yield very similar traces (recall that for each (x_s, θ) , $\check{U}(s; \theta, x_s)$ is a one-dimensional function of s), cf. figure 11. Finally, we note that none of the filtering steps explicitly filter on the sign of the perturbation – each frame selector will, in most circumstances, have roots which correspond to *positive*-valued quenching perturbations.

We initialize the continuation problem seeking solutions $(x_s, \check{U}(s; \theta, x_s))$ while controlling x_s , where θ is held constant. The continuation problem begins from the asymptotic case so that we may identify $\lim_{x_s \rightarrow \infty} U_s(s; x_s, \theta)$ uniquely. By treating the continuation with natural parameterization (i.e., not pseudo-arclength) we do not track solutions around curves where $x'_s = 0$; this is desirable since reversals in the branch would make the prediction of the critical amplitude non-unique for some x_s .

An additional benefit of the continuation problem is the comparison of sub-expressions from the asymptotic case to smaller perturbation widths. In figure 11, we show a diagnostic figure generated during the continuation process, which shows the perturbation, stable and unstable solutions, and the leading unstable left eigenfunction (left-most column), and a four-by-three block of diagnostic computations from the continuation. In the remainder of the figure we show $\check{\mu}_l(s; \theta, x_s)$ for each l (line, top row), and the roots of this function (black dots), while highlighting the asymptotic branch (colored dot). The second row shows the numerator of $\check{U}(s; \theta, x_s)$, likewise highlighting the roots of $\check{\mu}_l(s; \theta, x_s)$. The third row shows the denominator of $\check{U}(s; \theta, x_s)$, highlighting the roots of $\check{\mu}_l(s; \theta, x_s)$ and the asymptotic value. The final row shows the value of $\check{U}(s; \theta, x_s)$, highlighting the roots, and oscillating wildly for $x_s \ll L$ due to the division by near-zero values, i.e. $\langle \hat{\mathbf{w}}_1(\xi) | \check{\mathbf{X}}(\xi + s - \theta; x_s) \rangle \approx 0$. An animation of the continuation sequence is available here. However, in practice the asymptotic root is far from the regions where the denominator of (6) oscillates around 0, by construction, and the predictions do not suffer from numerical inaccuracies because of these far-field effects. Rather, as explained in the main text (16), we find some sensitivity to the curvature of $\check{U}(s; \theta, x_s)$ for $\check{\mu}_2(s; \theta, x_s)$ about s_3^* ; estimates of this factor are $|\partial_s^2 U(s_3^*)| \sim 10^{+2}$ and -10^{+5} in some cases.

REFERENCES

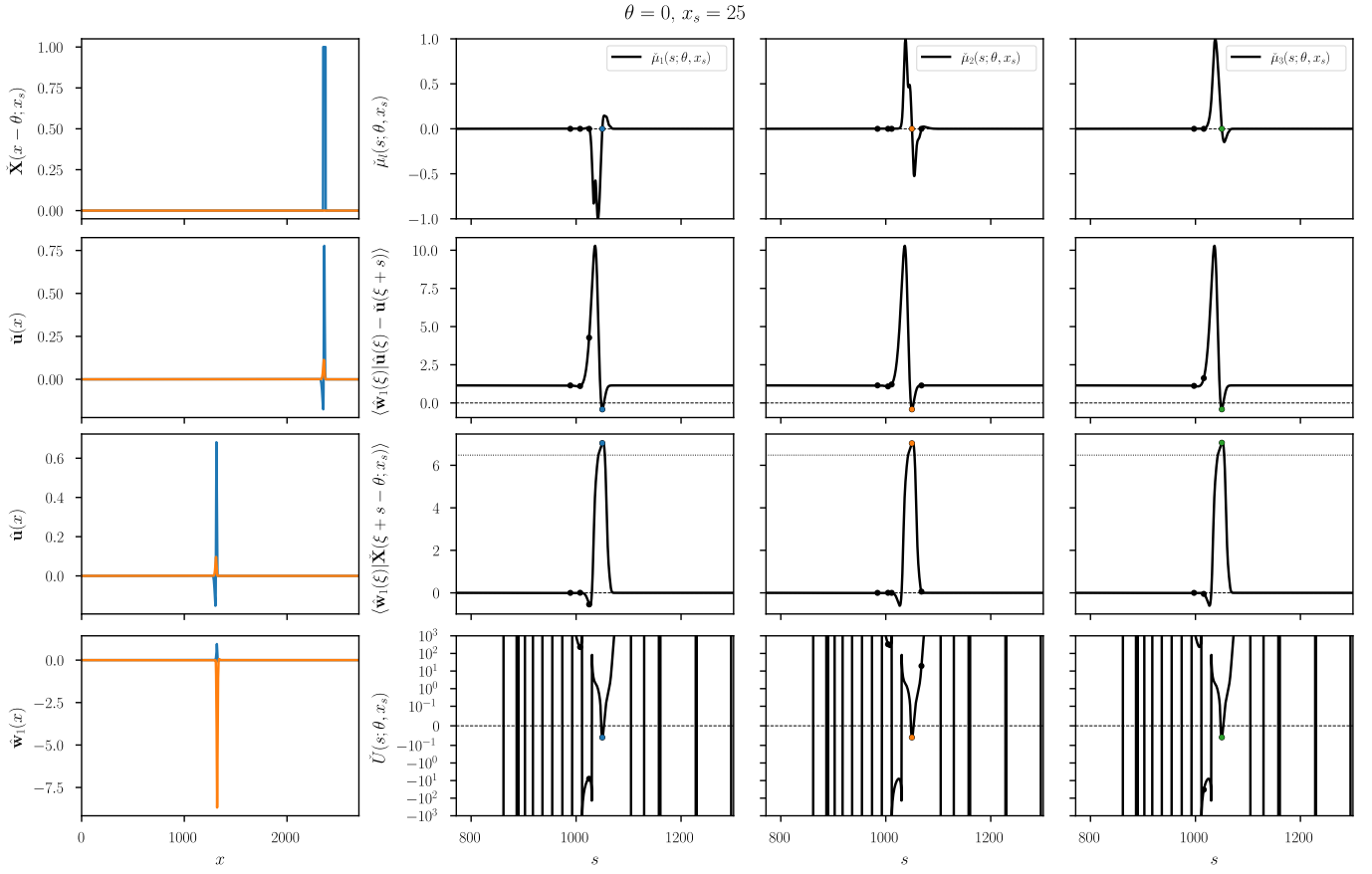


FIG. 11. Continuation to $x_s = 25$ for the quenching problem with $\theta = 0$ applied to the FitzHugh-Nagumo pulse with $\gamma = 0.025$. Note in the depiction of the denominator of $\tilde{U}(s; \theta, x_s)$ that the traced root is larger than the asymptotic (dotted line).

- [1] D. J. Dossall, V. G. Fast, and R. E. Ideker, **12**, 233.
- [2] F. H. Fenton, S. Luther, E. M. Cherry, N. F. Otani, V. Krinsky, A. Pumir, E. Bodenschatz, and R. F. Gilmour, **120**, 467.
- [3] P. Buran, M. Bär, S. Alonso, and T. Niedermayer, **27**, 10.1063/1.5010787, 29195336.
- [4] N. DeTal, A. Kaboudian, and F. H. Fenton, **119**, e2117568119.
- [5] G. V. Osipov and J. J. Collins, **60**, 54.
- [6] C. D. Marcotte and R. O. Grigoriev, **27**, 10.1063/1.5003259, 1703.10680.
- [7] V. N. Biktashev, **89**, 14.
- [8] C. Starmer, V. Biktashev, D. Romashko, M. Stepanov, O. Makarova, and V. Krinsky, **65**, 1775.
- [9] V. N. Biktashev and R. Suckley, **93**, 168103.
- [10] C. Starmer, **2**, 1848.
- [11] I. Idris and V. N. Biktashev, **76**, 1 ().
- [12] V. N. Biktashev and I. Idris, **35**, 311.
- [13] I. Idris and V. N. Biktashev, **101**, 244101 ().
- [14] B. Bezekci and V. N. Biktashev, **27**, 093916 ().
- [15] B. Bezekci and V. N. Biktashev, **80**, 104954 (), 1612.03502.
- [16] C. D. Marcotte and V. N. Biktashev, Physical Review E **101**, 042201 (2020).
- [17] R. Simitev and V. Biktashev, Bulletin of mathematical biology **73**, 72 (2011).
- [18] C. Marcotte, “Linear prediction,” https://github.com/cmarcotte/linear_prediction (2021), accessed: 2021-2-05.
- [19] E. J. Doedel, A. R. Champneys, F. Dercole, T. F. Fairgrieve, Y. A. Kuznetsov, B. Oldeman, R. Paffenroth, B. Sandstede, X. Wang, and C. Zhang, “Auto-07p: Continuation and bifurcation software for ordinary differential equations,” <https://github.com/auto-07p/auto-07p> (2007).
- [20] K. J. Burns, G. M. Vasil, J. S. Oishi, D. Lecoanet, and B. P. Brown, Physical Review Research **2**, 023068 (2020).
- [21] Reaction-diffusion models with pulse solutions may have a “one-dimensional spiral wave” [47] solution, which consists of repeated back-ignition and eventual self-interaction due to propagation around the periodic domain. Therefore two stable pulses traveling in opposite directions from the same original position can not interact destructively sooner than a significant proportion of $t > T$.
- [22] R. FitzHugh, Biophysical journal **1**, 445 (1961).
- [23] J. P. Keener, SIAM Journal on Applied Mathematics **39**, 528 (1980).

- [24] C. Rackauckas and Q. Nie, *Journal of Open Research Software* **5** (2017).
- [25] D. J. Gardner, D. R. Reynolds, C. S. Woodward, and C. J. Balos, *ACM Transactions on Mathematical Software (TOMS)* (2022), 10.1145/3539801.
- [26] A. C. Hindmarsh, P. N. Brown, K. E. Grant, S. L. Lee, R. Serban, D. E. Shumaker, and C. S. Woodward, *ACM Transactions on Mathematical Software (TOMS)* **31**, 363 (2005).
- [27] C. C. Mitchell and D. G. Schaeffer, *Bulletin of mathematical biology* **65**, 767 (2003).
- [28] F. Fenton and A. Karma, *Chaos: An Interdisciplinary Journal of Nonlinear Science* **8**, 20 (1998).
- [29] K. Nishi, S. Suzuki, K. Kayahara, M. Kuze, H. Kitahata, S. Nakata, and Y. Nishiura, *Physical Review E* **95**, 062209 (2017).
- [30] B. F. Farrell, *The Physics of fluids* **31**, 2093 (1988).
- [31] C. C. Pringle and R. R. Kerswell, *Physical review letters* **105**, 154502 (2010).
- [32] N. Chamakuri, K. Kunisch, and G. Plank, *Applied Numerical Mathematics* **95**, 130 (2015).
- [33] J. F. Whidborne and N. Amar, *BIT Numerical Mathematics* **51**, 447 (2011).
- [34] D. Lecoanet and R. R. Kerswell, *Physical Review E* **97**, 012212 (2018).
- [35] R. Matthysen and D. Huybrechs, **38**, A899.
- [36] S. L. Brunton, J. L. Proctor, J. N. Kutz, and W. Bialek, **113**, 3932, 1509.03580.
- [37] K. Hornik, M. Stinchcombe, and H. White, **2**, 359.
- [38] I. V. Biktasheva and V. N. Biktashev, **67**, 026221.
- [39] I. V. Biktasheva, A. V. Holden, and V. N. Biktashev, **16**, 1547 (), nlin/0504003.
- [40] I. V. Biktasheva, D. Barkley, V. N. Biktashev, G. V. Bordyugov, and A. J. Foulkes, **79**, 056702 ().
- [41] V. N. Biktashev, I. V. Biktasheva, and N. A. Sarvazyan, **6**, e24388.
- [42] S. R. Kharche, I. V. Biktasheva, G. Seemann, H. Zhang, and V. N. Biktashev, **2015**, 1.
- [43] T. A. Driscoll and N. Hale, *IMA Journal of Numerical Analysis* **36**, 108 (2014).
- [44] J. L. Aurentz and L. N. Trefethen, *SIAM Review* **59**, 423 (2017).
- [45] D. Collaboration, “Tau method,” https://dedalus-project.readthedocs.io/en/latest/pages/tau_method.html (2022).
- [46] U. M. Ascher, S. J. Ruuth, and R. J. Spiteri, *Applied Numerical Mathematics* **25**, 151 (1997).
- [47] E. N. Cytrynbaum and T. J. Lewis, *SIAM Journal on Applied Dynamical Systems* **8**, 348.